Recent advances in miniaturized optical gyroscopes

F. Dell'Olio Optoelectronics Laboratory, Politecnico di Bari, Via Orabona 4, 70125 Bari, Italy

T. Tatoli Optoelectronics Laboratory, Politecnico di Bari, Via Orabona 4, 70125 Bari, Italy

C. Ciminelli Optoelectronics Laboratory, Politecnico di Bari, Via Orabona 4, 70125 Bari, Italy
c.ciminelli@poliba.it

M. N. Armenise Optoelectronics Laboratory, Politecnico di Bari, Via Orabona 4, 70125 Bari, Italy

Low-cost chip-scale optoelectronic gyroscopes having a resolution $\leq 10^\circ$/h and a good reliability also in harsh environments could have a strong impact on the medium/high performance gyro market, which is currently dominated by well-established bulk optical angular velocity sensors. The R&D activity aiming at the demonstration of those miniaturized sensors is crucial for aerospace/defense industry, and thus it is attracting an increasing research effort and notably funds.

In this paper the recent technological advances on the compact optoelectronic gyroscopes with low weight and high energy saving are reviewed. Attention is paid to both the so-called gyroscope-on-a-chip, which is a novel sensor, at the infantile stage, whose optical components are monolithically integrated on a single indium phosphide chip, and to a new ultra-high Q ring resonator for gyro applications with a configuration including a 1D photonic crystal in the resonant path. The emerging field of the gyros based on passive ring cavities, which have already shown performance comparable with that of optical fiber gyros, is also discussed.
[DOI: http://dx.doi.org/10.2971/jeos.2014.14013]

Keywords: Optoelectronics, integrated optics, optoelectronic sensors, gyroscopes, ring resonators

1 INTRODUCTION

Since several decades, gyroscopes are routinely mounted on a wide range of vehicles such as military and civil airplanes, military ships, submarines, satellites, space launchers, and long-range ballistic missiles. All those applications, which are in the field of aerospace and defense, demand angular velocity sensors with a resolution $\leq 10^\circ$/h and a bias drift $< 1^\circ$/h. For example, attitude and orbit control of satellites for Earth observation/scientific mission and inertial navigation of submarines impose very stringent requirements in terms of bias drift and resolution, respectively of the order of 0.01°/h and 0.1°/h, while for applications such as autonomous navigation of rover vehicles and inertial navigation of missiles there are more relaxed requirements, i.e. bias drift in the range from 0.1°/h to 1°/h and resolution in the range from 1°/h to 10°/h [1, 2].

More recently other gyro application areas have emerged, i.e. robotics, medical instruments, automotive, and consumer applications. MEMS technology dominates those new markets assuring small device size, weight and fabrication cost [3]. Although continuous growth in the MEMS gyroscope market is expected along with their performance enhancement, reliability still remain a critical issue.

The application domains of angular velocity sensors with the required performance and the available gyro technologies are summarized in Figure 1.

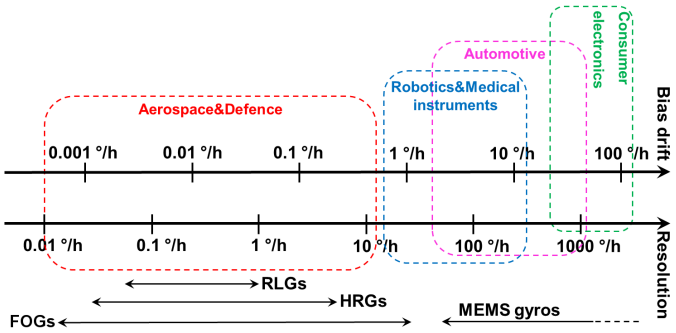

FIG. 1 Applications and requirements for different gyroscope technologies.

Almost half of the high-performance gyroscope market is covered by defense applications, while commercial aerospace represents the 25% of the market [4]. Currently these two market sectors are dominated by two well-established optoelectronic angular velocity sensor technologies, i.e. the optical technology, with Ring Laser Gyroscopes (RLGs) [5, 6] and Fiber Optic Gyroscopes (FOGs) [7]–[9], both based on the Sagnac effect [10], and the Hemispherical Resonator Gyroscopes (HRGs) [3, 11] based on the Coriolis force.

Received November 29, 2013; revised ms. received February 13, 2014; published March 11, 2014 ISSN 1990-2573

RLGs are robust devices, with no moving part and high resistance to vibrations and temperature gradients that can achieve high performance, i.e. resolution below 1°/h and bias drift better than 0.1°/h [5, 6]. These features make them suitable for applications demanding high and very high performance, especially in harsh environments. The RLG configuration includes either a triangular or a squared bulk optical cavity where a gaseous gain medium sustains the excitation of two optical waves propagating in the two opposite directions; at each corner of the cavity a high quality mirror is placed. When the device is rotating, a difference between resonance frequencies of the two modes arises, that is proportional to the rotation rate. Making one of the mirrors partially transmissive, a portion of each wave is extracted and sent to the read-out system that includes a prism, where the two extracted beams are combined, and a photodetector array, where the almost collinear beams exiting from the prism interfere to form a fringe pattern. Since the fringe pattern moves on the detector array surface in a direction depending on the sense of rotation, it is possible to determine the sign of the rotation rate. The angular velocity can be estimated by counting the intensity maxima in the fringe pattern.

The FOG is a phase sensitive device where the phase shift between two counter-propagating waves in a fiber coil is detected [7]–[9]. Its performance is similar to that of RLGs, i.e. bias drift ranging from 0.001°/h to 1°/h and resolution from 0.01°/h to 10°/h. These sensors have been utilized in several space missions such as Pleiades for the Earth observation [12], Aeolus for the observation of the atmospheric wind profile [13], and Planck to study the cosmic background radiation [14]. Due to the sensitivity to external perturbations (vibration transients, thermal and stress perturbations), FOGs cannot be extensively used for aircraft inertial navigation, due to a very harsh environment, while they are suitable for selected space applications where vibration and temperature transients are not so severe, even though attention will be paid to the ionizing radiation sensitivity.

Another kind of gyroscope that reaches the requirements for space applications is the Hemispherical Resonator Gyroscope (HRG). The recently launched Alphasat telecommunications satellite uses this kind of gyroscope for the attitude determination and control [15]. The sensing element of an HRG is a quartz hemispherical resonator with extremely high quality factor, up to 26 million [11]. Driving electrodes are used to excite a standing wave in the rim of the hemispherical resonator. In presence of rotation around the axis of the rim, nodes of the standing wave, otherwise fixed, rotate of an angle proportional to the rotation rate. The major disadvantage of this device, having a volume of several thousand of cm^3, is its high cost.

RLGs, FOGs, and HRGs are expensive bulk sensors with outstanding performance having weight, size, and power consumption which are incompatible with some key emerging applications such as attitude and orbit control of micro/nano satellites. In fact, those applications demand miniaturized gyroscopes with resolution around 10°/h or less, which are not available on the market. Available gyros with that value of resolution or even better, i.e. RLGs, FOGs and HRGs, have large weight and size, and high power consumption.

The development of a reliable and low-cost miniaturized gyroscope, having a minimum detectable angular velocity of the order of 10°/h, is a key technological challenge, which is motivating an increasing research effort. In literature at least three technological approaches have been proposed to face that challenge: the improvement of the MEMS gyros performance [16], the development of micro-gyros based on nuclear magnetic resonance (NMRG) [17], and the miniaturization of photonic gyros through integrated optical technologies, the so called gyroscope-on-a-chip (GoC) [18, 19].

While for MEMS gyroscopes the reliability issue is still open, and the NMRG, which exploits the shift of the Larmor precession frequency of nuclear spins to sense rotation, has serious critical aspect related to the complex fabrication technique and the sensitivity to magnetic fields, integrated optics allows the fabrication of gyros intrinsically immune to electromagnetic interference, with a very good resistance to harsh environments, and quite insensitive to vibrations.

In this work, chip scale optoelectronic gyroscopes are critically reviewed. An active optoelectronic gyroscope, using a semiconductor ring laser (SRL) as the source and the sensing element, was first proposed in [20] at the middle of '80s. In SRL-based gyros, mode competition and backscattering inside the optical cavity make quite complex the generation of the beating signal allowing the angular rate estimation. The Resonant Micro-Optic Gyro (RMOG) overcomes these effects by using a passive resonant cavity with high Q-factor. RMOGs based on either a silica-on-silicon ring resonator with very low loss or an InP resonator that allows the monolithical integration of all active and passive components on the same chip are discussed. A very innovative gyro configuration based on a ring resonator with a 1D photonic crystal (PhC) in the resonant path is also discussed. Moreover gyros using photonic structures including multiple ring resonators are reviewed.

2 SRL GYROSCOPES

The key component of the SRL gyroscopes is the ring laser, which is the element sensitive to rotation. SRL operates in single-longitudinal-mode conditions, exciting two lasing modes in the two opposite directions, clockwise (CW) and counter-clockwise (CCW). According to the Sagnac effect, in presence of a rotation around the normal to the plane of the ring cavity, the two beams propagate along different optical paths and, consequently, they have different resonance frequencies, ν_{CW} and ν_{CCW}. The difference $\Delta\nu = \nu_{CW} - \nu_{CCW}$, is proportional to the rotation rate Ω. For the circular ring laser it results in:

$$\Delta\nu = \frac{2R}{\lambda}\Omega = S\Omega \tag{1}$$

where $S = 2R/\lambda$ is the gyro scale factor, R is the ring radius and λ is the sensor operating wavelength.

Both performance and limitations of these gyros are strictly related to the SRL operating characteristics.

In a SRL the positive feedback is provided by a closed cavity that could have different shapes: circular, racetrack, squared, or triangular. In the design of both circular and racetrack SRLs attention must be paid to bending loss that increases when the curvature radius decreases. Conversely, squared and triangular SRLs, can provide lower loss [21].

Electrically pumped SRLs are fabricated in III-V semiconductors and their basic structure includes a substrate and a pn junction that encloses the active region. Usually the active region is formed by a graded-index separate confinement heterostructure in which there are single or multiple quantum well separated by barriers of graded-index. The advantage of this configuration is the possibility to separate the optical and the electrical confinements.

In the evolution of the SRL, attention was paid to the approach used to partially extract the beams generated within the laser cavity. In fact, the coupling mechanism affects the laser behavior, causing back-reflection in the cavity, so defining the portion of the light extracted from the cavity. The usable coupling techniques are: Y-junction, multimode interference (MMI) coupler and evanescent coupler. The first one has very strong intracavity back-reflection, while this is negligible in the case of the evanescent coupler, even if this latter requires a very accurate fabrication process because of the very small gap between the resonator and the waveguide. For the MMI coupler the fabrication tolerance is not so stringent and intracavity back-reflection is weak [22, 23].

In [24] the fabrication and the optical characterization of an SRL with a double quantum well GaAs/AlGaAs structure weakly coupled to a straight waveguide, is reported. The threshold current measured for this laser, having a radius of 1 mm, is 195 mA. At high injection current nonlinear effects arise due to self-saturation and cross-saturation effects in the gain medium, which, together with the mode competition effect and the lock-in effect, degrade the performance of the device.

A racetrack SRL with an S-section within the ring, as sketched in Figure 2, is reported in [25]. The cavity has a total length >10 mm and is fabricated on an InGaAs-GaAs-AlGaAs double-quantum-well heterostructure. The introduction of the S-section has the aim to provide unidirectional operation of the laser (see Figure 2) [26]. When forward biased, the S-section provides a nonreciprocal gain for the clockwise mode and the suppression of the undesired counter-clockwise mode.

The ultimate and unavoidable limit on the minimum detectable rotation rate, i.e. quantum limit, is caused by the laser spontaneous emission [27], which randomizes the phase of the electric field introducing uncertainty in the determination of the resonance frequency of each mode. The quantum noise limited minimum detectable rotation rate is given by:

$$\delta\Omega = \frac{\delta\nu}{S\sqrt{P_{OUT}}}\sqrt{\frac{Bhc}{\eta\lambda}} \qquad (2)$$

where P_{OUT} is the output laser power, $\delta\nu$ is the linewidth of the laser beams, B is the sensor bandwidth, η is the photodetector efficiency, λ is the laser operating wavelength. The sensor sensitivity could be increased using a large resonator, high output power or narrow laser emission linewidth.

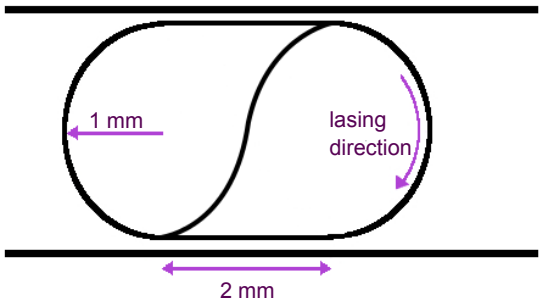

FIG. 2 Racetrack Semiconductor Ring Laser (SRL) with S section.

As a consequence of the lock-in effect, the evaluation of the rotation rate is not possible in the Ω range [$-\Omega_{lock-in}$, $+\Omega_{lock-in}$] where the two lasing modes are locked at the same frequency. In fact, due to the sidewall roughness of the ring a portion of each mode is backscattered. At low rotation rate this effect is very intense resulting in the coupling of the two modes. Such a phenomenon can be suitably described by the following equation that accounts for the phase (ψ) evolution of the two propagating modes inside the cavity:

$$d\psi/dt = S\Omega + b\sin(\psi) \qquad (3)$$

where b is the backscattering coefficient, which accounts for all the back-reflected light. At low rotation rate, the term $b\sin(\psi)$ is not negligible, and the equation has two stationary solutions with $d\psi/dt = 0$, i.e. the two propagating modes are locked at the same frequency.

As already mentioned, the idea of the SRL-based gyro was proposed in [20] for the first time. The configuration of that sensor includes the laser, with an InGaAsP active layer, and a Y output coupler. In [28], it is suggested the possibility to fabricate (on a single III-V semiconductor substrate) the ring laser integrated with two phase modulator operating in push-pull mode, in order to assure stable bidirectional operation of the laser, and an U-shaped output waveguide outcoupling a fraction of the optical power to a photodetector that detects the interference pattern of the two counter-propagating modes.

The design of the gyroscope sketched in Figure 3 [29, 30], was oriented to the optimization of the sensor footprint, an important feature for space applications [31]. An external SRL encloses an output coupler, two Y-junctions, and an MMI coupler, which allows the interference between the two counter-propagating lasing modes, and two photodetectors. The waveguides are fabricated in a GaAs/AlGaAs single quantum well structure. Both physical and geometrical parameters, such as number of quantum wells, Al concentration, doping concentration and ridge width were accurately modelled in order to reduce the laser threshold current and increase the efficiency, thus limiting loss and improving carrier confinement.

Another proposal of an SRL-based gyro on a single GaAs chip is described in [32]. Design criteria, fabrication and experimental characterization of the SRL are reported in [33], but

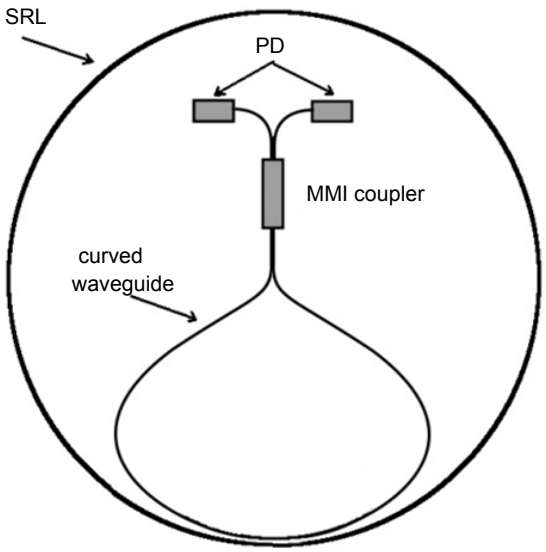

FIG. 3 Compact configuration of an SRL based gyro [29, 30] that includes an SRL inside of which there are a curved waveguide, an MMI coupler and two photodetectors for the system read-out.

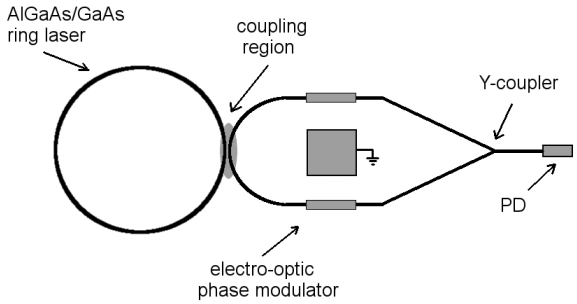

FIG. 4 Configuration of the SRL based gyro chip (3 mm x 5 mm) on GaAs [37].

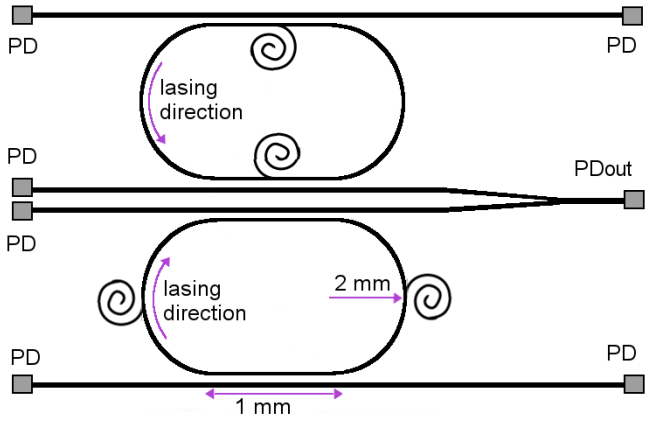

FIG. 5 Active gyroscope realized with two unidirectional racetrack SRL inside of which spiral waveguide sections prevent lasing in the undesired direction.

no beating frequency was measured from the device rotation treated up to $10^{9\circ}/\mathrm{h}$ [34].

The sensor proposed in [35] has the objective to simplify the gyro, detecting the Sagnac frequency difference directly from the voltage signal across the laser electrodes, thus avoiding the need of additional read-out components. To confirm this possibility, experiments have been conducted on a SRL gyro whose ring resonator is a fiber loop using a semiconductor optical amplifier (SOA). The minimum detected rotation rate reported is equal to $\sim 2\times 10^{3\circ}/\mathrm{h}$. Thus a proof of the direct proportionality between the applied mechanical rotation and the voltage across the SOA terminals was given. A theoretical analysis on the physical behavior of that device based on rate equations has been developed in [36].

The patented miniaturized integrated optical gyroscope in [37] has a footprint of 3 mm $\times$ 5 mm, including a double quantum well ring laser, a circular directional coupler, an electro-optic phase modulator, an Y-junction and a photodetector (see Figure 4). The two beams, allowing the angular velocity estimation, are generated by the ring laser, extracted by the coupler and interfere in the Y-junction, where the beating signal is generated. The electro-optic phase modulator operates in push-pull configuration adding a constant phase shift of $\pi/2$ to the two counter-propagating laser beams. This phase shift allows the detection of the sign of rotation. The choice of the material substrate (GaAs) is oriented to the reduction of the emission wavelength and the consequent scale factor improvement. The calculated shot noise limited resolution of that sensor is $0.01^\circ/\mathrm{h}$.

The backscattering induced lock-in and the mode competition make difficult the establishment of the laser bidirectional operation that is the basic requirement for the SRL-based gyro. A way to avoid these problems is presented in [38]. The configuration of this device is sketched in Figure 5. It includes two unidirectional racetrack shaped cavity lasers, with a total cavity length of 10.28 mm (1 mm radius of curvature and 2 mm long straight sections) and straight waveguides which are part of a Y-junction where the beams coming from the lasers are mixed and then detected by the photodetector $\mathrm{PD_{out}}$. Remaining photodetectors are used to monitor the suppression ratio of lightwaves in the undesired directions. As already mentioned, one possible way to achieve unidirectional operation is the introduction of an S-waveguide as sketched in Figure 2. An alternative option is the use of spiral absorbing elements (as shown in Figure 5) inside the laser cavity. In any case the beam in one direction experiences much higher loss than in the other.

No experimental evidence of the possibility of measuring rotation by those devices is available in the literature.

A different approach for the rotation measurement is presented in [39]. Here the sensing element is a circular Bragg laser in which two lasing beams propagate along a circular defect, with refractive index n_{def}, surrounded, on the opposite sides, by two Bragg reflectors formed by alternating layers with refractive indexes n_1 and n_2 (see Figure 6). An accurate design of a non-periodic index profile for the two Bragg reflectors allows good confinement of light in the guiding defect. In presence of a rotation the two counter-propagating beams exhibit not only a different resonance frequency, but also different Q-factor values. In particular, the beam that propagates in the opposite direction with respect to the rotation has a higher Q-factor than the other one. While the resonance frequency difference between the two counter-propagating beams is linearly proportional to the rotation, the Q-factor difference exhibits an exponential dependence on the rotation and, consequently, a gyroscope based on this laser could have a signifi-

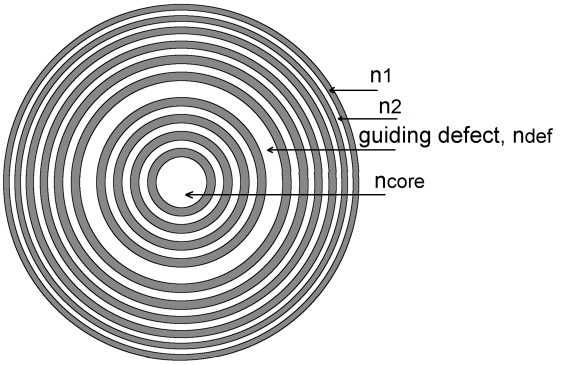

FIG. 6 Circular Bragg laser with a circular guiding defect, having refractive index n_{def}, surrounded by two Bragg reflectors in which dark rings have refractive index n_1 and white rings $n_2 < n_1$ [39].

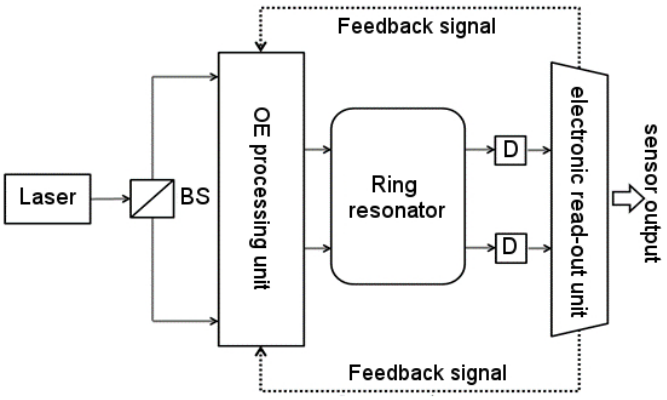

FIG. 7 Configuration of a Resonant Micro-Optic Gyroscope (RMOG), including a laser, a Beam Splitter (BS), Opto-Electronic (OE) components for signal processing, a ring resonator, two detectors (D) and an electronic read-out unit.

cantly enhanced performance. To our knowledge, that concept was never experimentally demonstrated.

In the last few years, the research effort on the SRL-based gyro was quickly decreasing due to some critical aspects of that device. We believe that only the identification of effective countermeasures mitigating lock-in and mode competition could allow the demonstration of the first prototype.

3 RESONANT MICRO OPTICAL GYROSCOPES (RMOGS)

Critical effects in SRL gyroscopes, i.e. backscattering, lock-in effect and mode competition, are intrinsically related to the SRL operation features. Therefore, they can be overcome by decoupling the laser source and the sensing element, as in the Resonant Micro-optic Gyroscope (RMOG), in which a passive ring resonator operates as the sensing element and an external laser source is used.

The configuration of an RMOG includes a narrow linewidth laser source, a high Q ring resonator, an optoelectronic processing unit, two photodetectors and an electronic read-out unit (see Figure 7). This sensor can be manufactured by using different technologies for each component: hybrid or monolithic integration. In the hybrid integration, it is possible to choose, for each component, the technology that assures the best performance, but the alignment of all components is difficult and the loss is larger. Monolithically integrated gyroscopes are surely more robust, compact and less power consuming.

In the RMOG, the rotation rate is measured by the difference between the resonance frequencies of the two counter-propagating beams injected into the high Q ring resonator. The ultimate limit on the measurement of the rotation rate is set by the shot noise at the photodetectors and is given by [40]:

$$\delta\Omega = \frac{1}{Qd\sqrt{P_{PD}}}\sqrt{\frac{2hc^3}{\lambda_0\eta\tau_{int}}} \qquad (4)$$

where d is the diameter of the ring resonator, Q its quality factor, λ_0 is the sensor operating wavelength, τ_{int} is the sensor integration time, P_{PD} is the power at the photodetector, η is the photodetector efficiency, h is the Planck constant, and c is the velocity of light in vacuum.

In addition to the unavoidable shot noise limit, RMOGs critical issues are the polarization fluctuations of the two modes propagating in the resonator, the backscattering effect, and the Kerr effect.

The key element of the system in Figure 7 is the ring resonator that strongly influences the gyro sensitivity. Currently ring resonators are considered fundamental building blocks for very large scale of integration (VLSI) photonics and a lot of components based on them, such as filters, wavelength division multiplexing systems, logic ports, modulators and lasers, have been demonstrated.

Different material systems are used for the fabrication of ring cavities. Silica-on-silicon and silicon nitride technologies allow the fabrication of resonators with very low loss [41]–[43], but $LiNbO_3$ [44], glass [45, 46], silicon [47], polymers [48], and InP [49, 50] are also used. Along with these fully passive ring resonators, some configurations, including an optical amplifier to compensate losses, have been also proposed and experimented [51, 52].

Gyroscope resolution can be enhanced through the use of ring resonators with very high Q-factors (see Eq. (4)). High Q values can be achieved by reducing ring resonator loss, mainly propagation loss and scattering loss due to roughness in waveguide sidewalls. To our knowledge, the best performing planar ring resonators are those ones reported in [41], fabricated in silica-on-silicon technology, and in [42, 43], fabricated in silicon nitride. In [41], measured propagation loss of a phosphorous doped silica-on-silicon ring resonator having a diameter of 6 cm, is equal to 0.0085 dB/cm and the resulting Q-factor is equal to 2.3×10^7. More recently high-Q Si_3N_4 ring resonators on silicon substrate have been reported. In [43], for a ring resonator with 7 μm core width, 45 nm core thickness, and 9.8 mm ring radius, a loaded Q-factor of 3.5×10^7 at 1550 nm has been measured, and the intrinsic Q-factor resulted to be 5.5×10^7.

Moreover, also microtoroids and wedge resonators have

demonstrated very high Q-factor. In particular, for the wedge resonator in [53], having a diameter of 7.5 mm, an ultra-high Q-factor equal to 8.75×10^8 has been experimentally demonstrated. The monolithic integration of this kind of resonant cavities with an input/output waveguide is a critical issue. In [54] a technique allowing the fabrication of a microtoroid and a bus straight waveguide monolithically integrated on a silicon chip is reported. With the proposed fabrication process, a microtoroid resonator, having a diameter equal to 70 μm, monolithically integrated with a bus waveguide has been demonstrated to have $Q = 3.2\times10^6$ at 1550 nm, and a Q value in excess of 4 million at 1330 nm. However, because of the complexity of the integration with other components, these structures cannot be considered as sensing element of the RMOGs.

3.1 RMOGs based on ultra-high Q silica-on-silicon ring resonator

RMOGs based on silica-on-silicon ring resonators have been extensively studied [55]–[58] and some prototypes [59] have been demonstrated. The main advantage of this technology is the very low waveguide propagation loss achievable, down to 0.01 dB/cm [41], which allows the fabrication of large ring resonators with Q-factor as high as 10^7 that is beneficial for the gyroscope resolution. For example an RMOG using the ring resonator investigated in [41], which has $Q = 2.3\times10^7$, would have a theoretical estimated shot noise limited resolution equal to 0.2°/h (with $P_{PD} = 1$ mW; $\eta = 0.9$; $\tau_{int} = 10$ s).

The possibility of using a silica-on-silicon resonator, as the sensing element in a passive optical gyro, was first demonstrated in [60], where the operation of an RMOG using a 5 cm diameter resonator, having a finesse of 10, was designed and experimentally investigated. The resolution was of the order of $10^{6\circ}$/h. Without the implementation of suitable countermeasures for fundamental noise sources, i.e. polarization fluctuations [61] and backscattering [62], which affect the rotation rate value adding an error that is higher than the shot noise, a good resolution in an adequate integration time cannot be achieved.

The aim of the approach in [63] was the integration on the same silica planar circuit of both the ring resonator and the optical components used to limit noise sources (Figure 8). The 14.8 cm long ring has a Q-factor = 2×10^6, with a waveguide propagation loss equal to 0.024 dB/cm. The integrated optical components for the noise mitigation are a silicon film that applies a pressure on the waveguide in order to reduce the polarization fluctuation effects and a thermo-optic modulator, operating in combination with a Mach-Zehnder interferometric switch, to implement the Binary Phase Shift Keying (B-PSK) modulation. However, because of their narrow bandwidth, thermo-optic phase modulators are not so efficient in reaching the carrier suppression, necessary to overcome the backscattering induced noise, at the right level [64].

Better performance can be reached by using $LiNbO_3$ phase modulators external to the chip for the phase modulation. Depending on the RF signal driving the modulator, different modulation techniques can be implemented: Single Phase

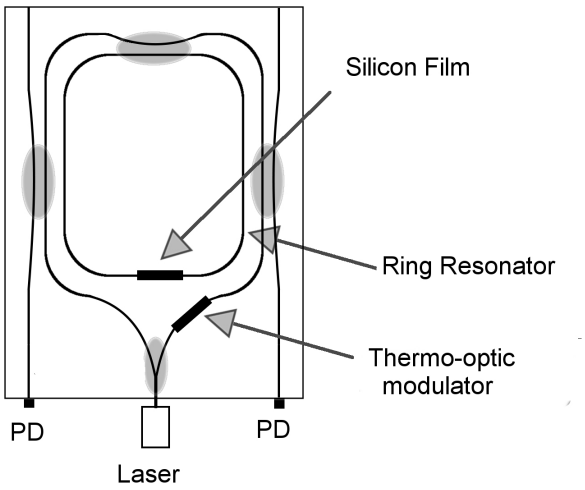

FIG. 8 Silica planar circuit including a ring resonator, a silicon film, a switch a thermo-optic modulator, and two photodetectors (PDs) [63].

Modulation Technique (SPMT) [62], Double Phase Modulation Technique (DPMT) [65], and Hybrid Phase Modulation Technique (HPMT) [66]. In the first case a couple of phase modulators, driven by sinusoidal signals at different frequencies, is used to achieve the suppression of the carrier components of the two counter-propagating beams [62, 64]. While this technique requires an accurate optimization of the modulation index, the DPMT has more relaxed constraints because two pairs of phase modulators in series are used to obtain additional carrier suppression [65]. In the last case the phase modulators are driven by signals, which are the sum of opposite slope triangle waves and sawtooth waves [66].

Another solution to improve the RMOG performance is based on the use of a spiral resonator, thus increasing the resonator optical path while maintaining a footprint close to 20 cm^2. Recently, a three loop spiral Ge-doped silica waveguide resonator, with the angle of the two crossing points close to 90° to reduce loss [67], has been characterized and its use as the sensing element of an RMOG has been also investigated [68].

The spiral resonator in [68], having a length of 42 cm, a footprint of 20 cm^2, propagation loss of 0.1 dB/cm, is evanescently coupled to two bus waveguides. The excess loss due to crossing points is < 0.01 dB. The experimental setup for its optical characterization includes a tunable laser, a polarization controller at the input of the sensing element used to select the eigenstate of polarization of the beams exciting the resonator, a thermoelectric cooler, keeping constant the temperature of the silica chip, and two photodetectors connected to an oscilloscope. A Q-factor of 1.5×10^6 has been calculated on the basis of the measured value of the full width at half maximum. The value of the estimated resolution is 156°/h, being the scale factor equal to 2.88×10^4, the photodetector efficiency 0.9, the integration time 1 s and the measured power at the photodetector equal to 10 μW. This last value is so low because of the high loss due to the fabrication process and coupling interfaces experienced by the optical beams in their propagation from the laser source to the photodetectors. Improving this value up to 2.4 mW, the target resolution of 10°/h has been calculated,

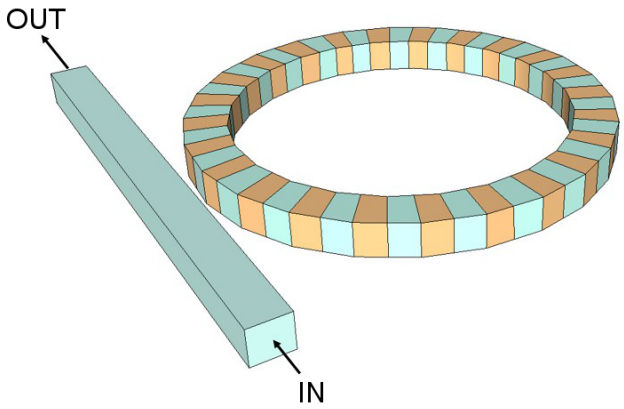

FIG. 9 Configuration of the ring resonator with a 1D PhC included in the resonant path.

while maintaining the same footprint. The estimated bias drift of that sensor is equal to 0.2°/h.

In order to maximize the Q-factor of the RMOG sensing element, resonators with loss compensation have also been investigated, as already mentioned. In the configuration proposed in [51], two SOAs are hybridly integrated, in symmetrical positions within the resonator, in order to fully compensate propagation loss. A Q-factor of 2.9×10^8 and a minimum detectable rotation rate of 0.2°/h can be predicted for the resonator having a length equal to 94.8 mm. Critical issues of this configuration arise from nonlinear effects that make complex its control. Another type of compensated resonator is investigated in [52]. The proposed racetrack cavity is fabricated by using an active waveguide in neodymium doped glass. A Q-factor of 1.9×10^7 is reached for the resonator having a length of 56 mm.

An alternative RMOG configuration is proposed in [69]. That sensor is based on two ring resonators that are fabricated independently and then bonded back-to-back into one chip. The aim of this approach is the reduction of the backscattering, Kerr effect and the polarization fluctuation induced noise. Since only one beam propagates in each resonator, there is not interference between backscattered light and propagating beam. The performance of that device is not mentioned by the authors.

A very innovative approach for the enhancement of the Q-factor in ring resonators for gyro applications, is described in [70], where a 1D PhC is included in the resonant path of a circular ring cavity. A possible realization of that idea is a ring resonator in silica-on-silicon technology having a diameter of 4.59 cm, weakly coupled to a straight bus waveguide (coupling efficiency about 2%). The resonant path includes a low-index-contrast Bragg grating extending over all its length that could be fabricated by an appropriate UV writing technique (see Figure 9). Assuming that the guiding structure has a propagation loss of 0.07 dB/cm, a Q-factor of about 7×10^9 has been calculated for that resonant device.

Basic features of the RMOGs based on silica-on-silicon resonators with the best shot noise limited resolution are summarized in Table 1. The gyro with the best experimentally measured performance is reported in [65, 71]. The configuration of this RMOG includes a fiber laser, whose frequency is locked to the resonance frequency of the CW resonant mode, two couples of phase modulators implementing double phase modulation technique, the sensing element and other opto-electronic components. The sensing element is a polarization maintaining silica waveguide ring resonator having a diameter of 2.5 cm and a Q-factor of 3×10^6. The double phase modulation scheme has allowed the reduction of the short term bias stability down to 38°/h, for an observation time of 60 s and an integration time of 10 s. The minimum detectable rotation rate was about 400°/h [65]. With the same device a long term bias stability of 800°/h for 1 h observation time is obtained.

At this stage of their development, RMOGs based on silica-on-silicon cavities exhibit performance which is still far from that are demanded by aerospace and defence industry. They could be used in automotive and consumer electronics where the low-cost MEMS gyros already dominate. Therefore only after the enhancement of their performance of one/two order of magnitude, those RMOGs could have a role in the gyro market. We believe that RMOGs based on a cavity including a Bragg grating in the resonant path will have a disruptive impact on the market if their performance will be experimentally confirmed.

3.2 InP based gyro on a chip

While giving the opportunity to make the best technological choice for each component of RMOGs, the hybrid integration imposes tight requirements on the alignment of number of opto-electronic components. The alternative technological solution, i.e. the monolithic integration of all gyro optoelectronic components on the same substrate, can provide higher compactness of the device and improved immunity to external disturbances. The III-V semiconductor technology is the only one that could allow the fabrication of a GoC, which includes all active and passive components on the same substrate thus enhancing the scaling of the optical resonant gyroscopes.

The key element of the fully integrated RMOG remains the ring resonator, whose size and performance determine the gyro resolution: the product between the resonator Q-factor and its diameter is inversely proportional to the minimum detectable rotation rate (see Eq. (4)). As described in [49], a ring resonator with $Q \geq 10^6$ and $d \geq 10$ mm is necessary to achieve a resolution of $\delta\Omega = 10°/\text{h}$ or less.

Although ring resonators have been demonstrated both in $In_{1-x}Ga_xAs_yP_{1-y}$/InP and in GaAs/$Al_xGa_{1-x}As$ system, the research effort has been focused on the InP based material since it exhibits lower loss. However, since in $In_{1-x}Ga_xAs_yP_{1-y}$/InP waveguides propagation loss is typically higher than 1 dB/cm, which does not allow to achieve a required Q value $\geq 10^6$, the optimization of the waveguide design and improvement of the technological process still remains an important goal.

The design, fabrication and characterization of a ring resonator with radius of 13 mm, coupled to a single bus waveguide and fabricated with low loss InGaAsP/InP rib waveg-

Authors	Resonator footprint (cm^2)	Resonator Q-factor	Measured Short term bias stability (τ_{int} = 10 s) (°/h)	Measured long term bias stability (observation time 1 h) (°/h)	Theoretically estimated bias stability (°/h)	Shot noise limited resolution (*) (°/h)	Measured resolution (°/h)
Ma et al., Mao et al. [65, 71]	6.25	3×10^6	40	800	-	5	400
Feng et al., Lei et al. [66, 72]	16	7×10^6	800	1800	-	1	-
Ciminelli et al. [68]	20	1.5×10^6	-	-	0.2	5	-
Ciminelli et al. [70]	21	7×10^9	-	-	-	< 0.01	-

* Theoretical value with P_{PD} = 1 mW; η = 0.9; τ_{int} =10 s.

TABLE 1 Basic feature of the best performing RMOGs based on silica-on-silicon ring resonators.

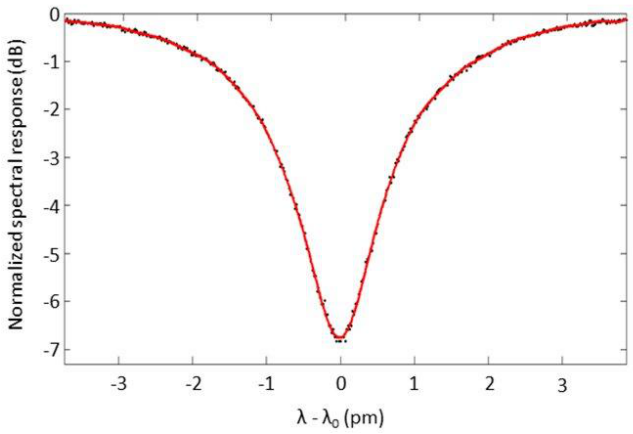

FIG. 10 Spectral response of the ring resonator having radius 13 mm, coupled to a single bus waveguide from which is separated by a 1524 nm gap; this resonator has a quality factor of 0.97×10^6. Reprinted from Ref. [50] with permission of OSA 2013.

uide are reported in [73, 50]. For the realized rib waveguide, with an etch depth of 0.3 μm and a width of 2 μm, a propagation loss for the fundamental quasi-TE mode reaching the record value of 0.45 dB/cm has been measured.

Using an experimental setup that includes a tunable laser and a photodetector connected to an oscilloscope, the resonator spectral response has been measured (see Figure 10). The resonator has a quality factor equal to 0.97×10^6 [50]. If it is used as the sensing element of an RMOG, the target resolution of 10°/h can be reached with an average power at photodiodes input equal to 13.84 mW. In addition to the increase of the power at photodiodes, in order to obtain better performance, a further decrease of the propagation loss is required or a larger resonator must be used. Unfortunately, this last choice implies an increase of the chip footprint with negative consequence on the uniformity of the technological process.

We believe that the GoC concept is very promising and attractive, although its experimental demonstration demands an additional notably technological effort.

3.3 RMOGs read-out

The RMOGs read-out system has a crucial role in RMOGs, being the frequency difference between the two counter-propagating resonant modes ($\Delta\nu = \nu_{CW} - \nu_{CCW}$), from which the measure of the rotation rate is extracted, very little, of the order of 1 Hz. Moreover, an efficient signal processing technique must be implemented in order to distinguish the rotation induced $\Delta\nu$ from the noise sources, such as backscattering induced noise [62, 64, 65], laser frequency noise [74], and fluctuations of the resonance frequency of the resonator mainly due to the temperature drift [75].

Among several configurations proposed for the read-out, basically two options are possible, i.e. phase or frequency modulation of the optical signals exciting the ring resonator. Due to its simplicity, the first technique is the most common. In both cases the read-out circuit can be designed in either open or closed loop configuration.

The configuration of the read-out system using phase modulation technique is depicted in Figure 11. The signal from the laser source is split by the beam splitter (BS). Before entering the resonator cavity, the two beams are phase modulated by the two phase modulators PM1 and PM2 and frequency shifted by the acousto-optic frequency shifters AOM1 and AOM2. At this point the amplitude of the two beams entering the resonator in the CW and CCW direction ($E_{in,CW}$ and $E_{in,CCW}$), can be written as:

$$\begin{aligned} E_{in,CW} &= \frac{E_0}{\sqrt{2}} \exp^{i[2\pi(\nu_0+\delta\nu_1)t + M\sin(2\pi f_1 t)]} \\ &\cong \frac{E_0}{\sqrt{2}} \exp^{i2\pi\nu_1 t} \sum_{k=2}^{2} J_k(M) \exp^{i2\pi f_1 t} \\ E_{in,CCW} &= \frac{E_0}{\sqrt{2}} \exp^{i[2\pi(\nu_0+\delta\nu_2)t + M\sin(2\pi f_2 t)]} \\ &\cong \frac{E_0}{\sqrt{2}} \exp^{i2\pi\nu_2 t} \sum_{k=2}^{2} J_k(M) \exp^{i2\pi f_2 t} \end{aligned} \quad (5)$$

where E_0 and ν_0 are the intensity and the emission frequency

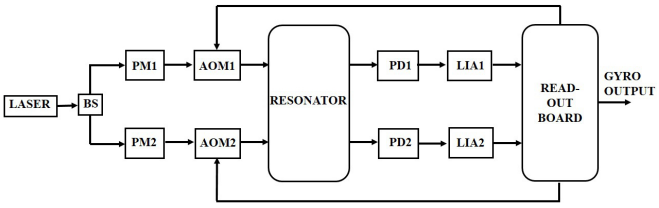

FIG. 11 Configuration of read-out architecture based on phase modulation spectroscopy technique in closed-loop configuration. (BS beamsplitter, PM phase modulator, AOM acousto-optic modulator, PD photodetector, LIA lock-in amplifier).

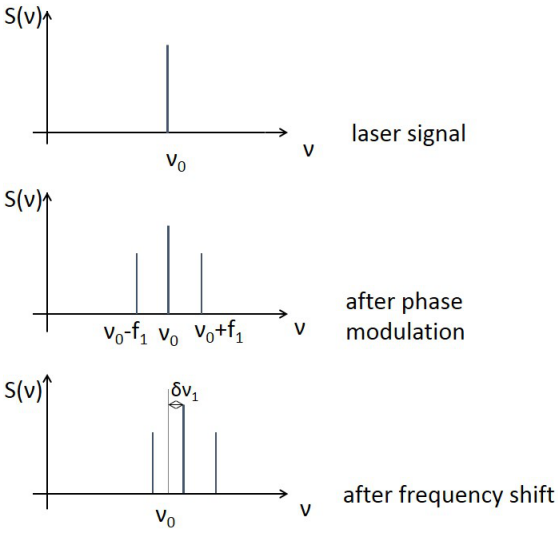

FIG. 12 Spectra of generated, phase modulated and frequency shifted laser signal ($\nu$is the frequency and $S(\nu)$ is the power spectral density).

of the laser source, respectively, $\delta\nu_{1,2}$ are the frequency shifts due to AOM1 and AOM2, $\nu_{1,2} = \nu_0 + \delta\nu_{1,2}$ are the frequencies of the beams entering the resonator, $f_{1,2}$ and M are the phase modulation frequencies and the modulation index of PM1 and PM2, respectively. Under the assumption that the phase modulation index (related to the amplitude of the sinusoidal modulating signal and to the half-wave voltage of phase modulators, $M = \pi V/V_\pi$) is close to 1, the two equations can be approximated by the series expansion, with k the index of the summation and J_k the Bessel functions of the first kind. As a consequence of the phase modulation, spectral components at $\nu_0 \pm f_{1,2}$ and $\nu_0 \pm 2f_{1,2}$ appear, and these components, with the original one at ν_0, are all shifted by AOMs, as it is schematically shown in Figure 12.

After exciting the cavity, the amplitudes of the beams at the output of the sensing element are given by:

$$E_{out,CW} = \frac{E_0}{\sqrt{2}} \exp^{i2\pi\nu_1 t} \sum_{k=-2}^{k=2} J_k(M) H(\nu_1 + kf_1) \exp^{i2\pi f_1 t}$$
$$E_{out,CCW} = \frac{E_0}{\sqrt{2}} \exp^{i2\pi\nu_2 t} \sum_{k=-2}^{k=2} J_k(M) H(\nu_2 + kf_2) \exp^{i2\pi f_2 t} \quad (6)$$

where H is the resonator spectral response having a Lorentzian-like shape. These two signals are sent to the photodetectors whose outputs are voltage signals that can be

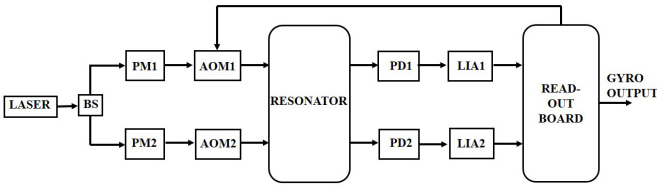

FIG. 13 Configuration of the read-out architecture based on phase modulation spectroscopy in open-loop configuration. (BS beamsplitter, PM phase modulator, PD photodetector, LIA lock-in amplifier).

written as:

$$D_{CW} = Z_{PD}R_{PD}\left|\frac{E_0}{\sqrt{2}}\sum_{k=-2}^{k=2} J_k(M)H(\nu_1 + kf_1)\exp^{i2\pi f_1 t}\right|^2 \cong \frac{Z_{PD}R_{PD}E_0}{\sqrt{2}}[A_1 + B_1\cos(2\pi f_1 t) + C_1\cos(4\pi f_1 t)]$$
$$D_{CCW} = Z_{PD}R_{PD}\left|\frac{E_0}{\sqrt{2}}\sum_{k=-2}^{k=2} J_k(M)H(\nu_2 + kf_2)\exp^{i2\pi f_2 t}\right|^2 \cong \frac{Z_{PD}R_{PD}E_0}{\sqrt{2}}[A_2 + B_2\cos(2\pi f_2 t) + C_2\cos(4\pi f_2 t)] \quad (7)$$

where

$$A_j = J_0^2(M)H^2(\nu_j) + J_1^2(M)[H^2(\nu_j + f_j) + H^2(\nu_j - f_j)]$$
$$B_j = 2J_1(M)J_0(M)H(\nu_j)[H(\nu_j + f_j) + H(\nu_j - f_j)]$$
$$C_j = -2J_1^2(M)H(\nu_j + f_j)H(\nu_j - f_j) \quad (8)$$

$j = 1, 2$, and Z_{PD} and R_{PD} are the impedance and the responsivity of the photodetectors, respectively.

The signals go from the photodiodes to the two lock-in amplifiers $LIA_{1,2}$. LIAs, which are driven by the same signals driving the two phase modulators, have an output that is a DC voltage level proportional to the amplitude of the harmonic component at frequencies $f_{1,2}$. When the frequencies of the two beams, $\nu + \delta\nu_{1,2}$, are equal to the resonant frequencies of the resonator in the two directions, the coefficient B_j is equal to 0, being H a symmetrical function, so the LIAs outputs are null. On the contrary if this condition is not satisfied the LIAs outputs are proportional to the harmonic components at frequencies $f_{1,2}$.

In the closed loop configuration the two LIAs output signals are used to lock, by means of the two AOMs, the central frequency of each beam entering the resonator ($\nu_{1,2}$) to the resonant frequencies ν_{CW} and ν_{CCW}, so that the difference between AOMs driving signals is the gyro output (see Figure 11). In this case, a single frequency laser source can be used. On the contrary, in the open loop configuration (see Figure 13) there is only one feedback loop used to lock the laser frequency to one of the two resonant frequencies. However, in this case, the sensor sensitivity results degraded.

Research effort on the read-out system has to be spent for the RMOG technology development. Several research groups are already working on this topic since several years and the achieved results appear to be very promising.

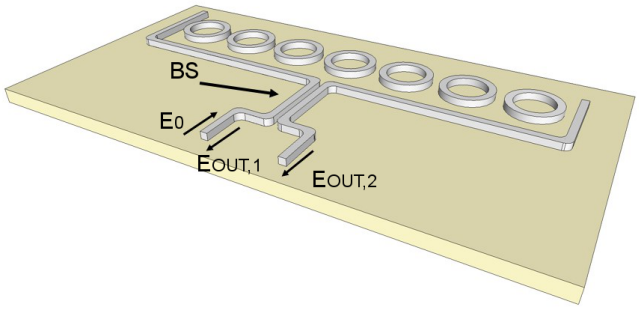

FIG. 14 Configuration of a CROW based gyro: the input optical beam (with amplitude E_0) is split by a beam splitter (BS) and the two beams are coupled to the CROW where they counter-propagate before being recombined in the BS. At the output the two beams $E_{OUT,1}$ and $E_{OUT,2}$ are obtained.

4 MULTI RING CONFIGURATION FOR ANGULAR VELOCITY SENSOR

Multi ring optical cavities as sensing elements of angular velocity sensors, have attracted some interest in recent years, because their large structural dispersion could enhance the Sagnac phase shift [75, 76]. Coupled Resonator Optical Waveguide (CROW) structures [78], in which high-Q resonators are coupled each other via evanescent fields, can be used as the basic building block of a gyroscope having the configuration shown in Figure 14.

According to [79] when two optical beams counter-propagate in the rotating CROW, the Sagnac phase shift $\Delta\Phi$ that they accumulate is given by:

$$\Delta\Phi = \frac{n_g}{n_0}\Delta\phi \tag{9}$$

where $\Delta\phi$ is the Sagnac phase shift suffered by the beams in a single ring, n_g is the CROW group index and n_0 is the refractive index of the rings. Since the CROW group index can be very high, $\Delta\Phi$ may be larger than $\Delta\phi$. After the propagation, the two beams are combined in a 3-dB coupler and the measure of the rotation rate is extracted by comparing the intensity of beams coming out from the coupler.

Different configurations of multi-ring based gyros have been proposed. In [78] a CROW structure with identical ring resonators, arranged along an arc, is suggested (Figure 15(a)). Two resonators are coupled to two curved waveguides ending in a 3 dB beam splitter from which the interference signal of the two counter-propagating optical beams is obtained. A slightly different configuration is proposed in [80] (Figure 15(b)) where two nested ring resonators, having different radius, are coupled each other and the external one is coupled to a bus waveguide. Both gyro configurations are phase-sensitive.

Multi ring optical cavities impose severe fabrication requirements related to resonator size and loss. Fabrication process must ensure an accurate control on the ring radius and the gap between coupled resonators or between the resonators and the bus waveguides. Loss must be minimized since a very high Q-factor ($\geq 10^7$ [78]) is required for micrometer size resonators. In literature [81] a comparison between performance of the Resonant FOG and the multi ring based gyro has been

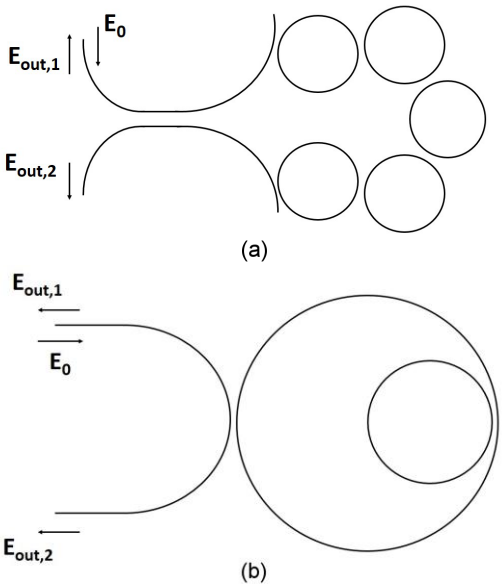

FIG. 15 Different configuration of multi ring structures proposed as sensing element of gyro: (a) CROW structure with five identical ring resonators, and (b) folded structure with two nested ring resonator having one the half radius of the other.

reported together with some criticisms about the effectiveness of enhancing the Sagnac phase shift in a multi ring structure.

In [82, 83] the impact of chirped CROW on the performance of a gyro is analyzed. In [82] a comparison between the spectral response of an array of identical resonators and an array of resonators that have different dimensions is reported. In particular, the proposed configuration includes an odd number of resonators, arranged in a symmetrical way. From the smaller one at the center of the array to those at the edge, lengths are increased of an integer number of wavelength. The transmission spectrum of this chirped CROW has a larger bandwidth with peaks of transmission isolated and enhanced with respect to the standard CROW. In this way it is possible to obtain a higher sensitivity of the gyro without increasing the resonators number. In fact, in [82], the authors state that the one wavelength chirped structure with 5 resonators has a sensitivity equal to an un-chirped structure including 35 resonators. Moreover, when coupling coefficients between resonators are chirped, instead of their length, the spectral response exhibits a sharper transmission resonance. This would allow the design of a phase sensitive gyro with a resolution of $0.002^\circ/h$ and a footprint area of 0.16 mm [83].

An alternative approach, with respect to the phase sensitive CROW based gyro described above, is suggested in [84], where a frequency sensitive gyro based on a multi ring structure is investigated. The advantage of this configuration is the enhancement of the scale factor, keeping equal footprint, with respect to an RMOG with a single resonator. As sketched in Figure 16 the structure analyzed includes three ring resonator having different radius. Two counter-propagating beams are injected in the triple ring resonator through a straight waveguide. After resonating, the two beams are extracted from the other straight waveguide. The central resonator has a radius much lower than others, while the difference between the other two radii is very small. The coupling coefficient be-

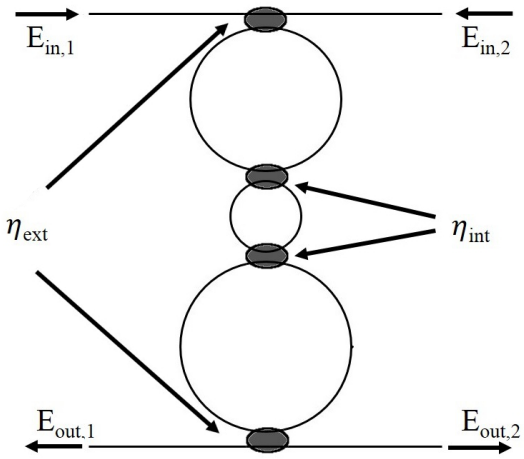

FIG. 16 Triple ring resonator configuration with two bus waveguides used to inject counter-propagating beams ($E_{in,1}$, $E_{in,2}$) and extract output beams ($E_{out,1}$, $E_{out,2}$) respectively.

tween the inner resonators (η_{int}) and the coupling coefficient between the external resonators and the bus waveguides (η_{ext}) are different. On the basis of numerical analysis, it has been concluded that an enhancement of the sensor scale factor can be obtained only if $\eta_{ext} > \eta_{int}$. The ratio η_{ext}/η_{int} must be tuned in a way that assures the maximum enhancement without a significant increase of η_{int} that can degrade the Q-factor of the resonators. With the suitable optimization of rings radii and coupling coefficients, it is possible to obtain an enhancement of the gyro sensitivity without increasing its footprint. Considering resonators with Q-factor as high as 10^6, a footprint reduction of about 1.88 can be obtained in the triple resonators structure with respect to the case of a single resonator device.

5 CONCLUSIONS

The very promising research field of integrated optical gyroscopes is reviewed in this paper. Aiming at the development of an optoelectronic ultra-compact gyro having performance and reliability compliant with the requirements of aerospace and defense industry, five technological approaches have been explored, i.e. the SRL-based gyros, the RMOGs based on ultra-high Q silica resonators, the InP gyroscope-on-a-chip, the gyro configuration based on the ring cavity with a Bragg grating in the resonant path, and the gyros based on multi-rings cavities. All those devices have been critically discussed; modulation techniques to improve the gyro resolution have been also described. Advantages, critical aspects, theoretical/experimental performance of each technology are summarized in Table 2. We expect that a gyroscope-on-a-chip prototype will be developed in the next few years. If the characterization/qualification of that prototype will be successful we believe that the gyroscope-on-a-chip will have a very notably impact on the market of the angular velocity sensors with a resolution of the order of 10°/h or less. Prototypes of RMOGs based on silica resonators have been already reported by several research group but the experimentally demonstrated performance is still at least one order of magnitude worse than that one demanded by applications in the field of aerospace and defense and thus an improvement of those gyros is needed to realize a significant impact on the market. Due to lock-in and mode competition SRL-based gyros are still far from the prototyping stage while gyros based on either multi-rings cavities or rings including a 1D PhC in the resonant path seem to be promising, although further theoretical/experimental efforts are necessary to evaluate those technological approaches.

We believe that in the next years the research effort will be focused on the RMOGs. The technological activity will aim at both the demonstration of cavities having an ultra-high Q-factor and the improvement of the integration techniques enabling the fabrication of the InP GoC. An in depth theoretical work on the most innovative cavities for gyroscopic applications, i.e. the multi-ring configuration and the resonator including the 1D PhC, is also expected.

References

[1] N. Barbour, and G. Schmidt, "Inertial sensor technology trends," IEEE Sens. J. **1**, 332–339 (2001).

[2] M. N. Armenise, C. Ciminelli, F. De Leonardis, R. Diana, V. Passaro, and F. Peluso, *Gyroscope technologies for space applications* (4th Round Table on Micro/Nano Technologies for Space, Noordwijk, 20–22 May 2003).

[3] K. Liu, W. Zhang, W. Chen, K. Li, F. Dai, F. Cui, X. Wu, et al., "The development of micro-gyroscope technology," J. Micromech. Microeng. **19**, 113001 (2009).

[4] "Gyroscopes and IMUs for defense, Aerospace & Industrial," Yole Development Report (2012), http://www.reportlinker.com/p01008831-summary/Gyroscopes-and-IMUs-for-Defense-Aerospace-Industrial.html

[5] W. W. Chow, J. Gea-Banaloche, L. M. Pedrotti, V. E. Sanders, W. Schleich, and M. O. Scully, "The ring laser gyro," Rev. Mod. Phys. **57**, 61–104 (1985).

[6] F. Aronowitz, "Fundamentals of the ring laser gyro," in *Optical gyros and their applications*, D. Loukianov, R. Rodloff, H. Sorg, B. Stieler, eds., (Canada Communications Group, Quebec, 1999).

[7] B. Culshaw, and I. P. Giles, "Fibre optic gyroscopes," J. Phys. E: Sci. Instrum. **16**, 5–15 (1983).

[8] H. C. Lefèvre, "Fundamentals of the interferometric fiber-optic gyroscope," Opt. Rev. **4**, 20–27 (1997).

[9] B. Culshaw, "The optical fibre Sagnac interferometer: an overview of its principles and applications," Meas. Sci. Technol. **17**, R1–R16 (2006).

[10] E. J. Post, "Sagnac effect," Rev. Mod. Phys. **39**, 475–493 (1967).

[11] P. Pai, F. K. Chowdhury, C. H. Mastrangelo, and M. Tabib-Azar, "MEMS-based hemispherical resonator gyroscopes," in *Proceedings to the IEEE Sensors Conference*, 1–4 (IEEE, Taipei, 2012).

[12] M. A. Gleyzes, L. Perret, and P. Kubik, *Pleiades architecture and main performances* (XXII Congress of the International Society for Photogrammetry and Remote Sensing, Melbourne, 25 August–1 September 2012).

[13] ADM-Aeolus (Atmospheric Dynamics Mission) https://directory.eoportal.org/web/eoportal/satellite-missions/a/adm-aeolus

[14] D. Zorita, A. Agenjo, S. Llorente, G. Chlewicki, A. Cocito, P. Rideau, S. Thuerey, et al., *How Planck AOCS behaved, commissioning early*

Technology	Advantages	Critical aspects	Shot noise limited theoretical resolution	Experimental performance
Monolithic GaAs configuration based on a SRL [37] 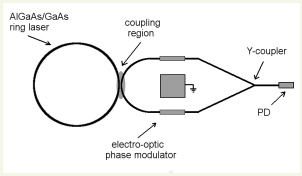	• Simple configuration including a few optoelectronic components • Simple read-out circuit	• Lock-in • Mode competition • Rotation-induced beating signal never experimentally observed	<0.1°/h	–
RMOGs based on ultra-high *Q* Silica-on-Silicon resonators [65, 71] 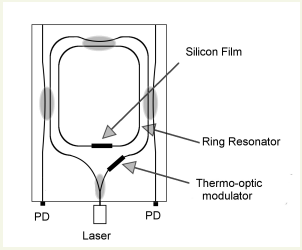	• Decoupling of the laser and the sensing element • Hybrid integration allowing the selection of the best technology for each component	• Relative complexity of the configuration including more than ten optoelectronic components	<10°/h	Resolution about 400°/h Short term bias drift = 40°/h [71]
InP gyroscope-on-a-chip [50] 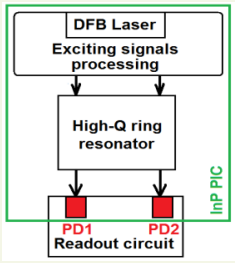	• The monolithic integration enhances the device compactness and immunity to external disturbances (e.g., vibrations)	• No experimental demonstration	10°/h	–
Gyro configuration based on a ring resonator with a 1D PhC included in the resonant path [70] 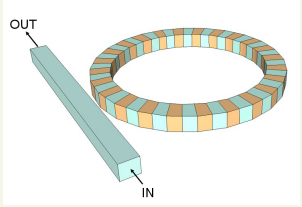	• Extremely high Q factor of the cavity • Very good expected resolution (close to that one of RLG and FOG)	• No experimental demonstration	<0.01°/h	–
Gyro based on multi-rings cavities [78] 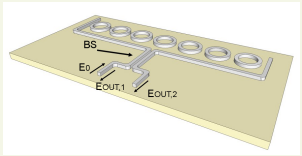	• Good performance/ footprint ratio	• No experimental demonstration	<0.1°/h	–

TABLE 2 Advantages, critical aspects, theoretical/experimental performance of the different integrated optical gyroscope technologies.

orbit and pointing manoeuvres (8th International ESA Conference on Guidance, Navigation & Control Systems, Karlovy Vary, 2011).

[15] Alphasat I/Inmarsat-XL (Inmarsat-Extended L-band Payload) https://directory.eoportal.org/web/eoportal/satellite-missions/a/alphasat

[16] M. F. Zaman, A. Sharma, Z. Hao, F. Ayazi, "A mode-matched silicon-yaw tuning-fork gyroscope with subdegree-per-hour allan deviation bias instability," IEEE J. Microelectromech. Syst. **17**, 1526–1536 (2008).

[17] E. A. Donley, "Nuclear magnetic resonance gyroscopes," in *Proceedings to the IEEE Sensors Conference*, 17–22 (IEEE, Kona, 2010).

[18] M. N. Armenise, C. Ciminelli, F. Dell'Olio, and V. M. N. Passaro, *Advances in gyroscope technologies* (Springer-Verlag, Heidelberg, 2010).

[19] C. Ciminelli, F. Dell'Olio, C. E. Campanella, and M. N. Armenise, "Photonic technologies for angular velocity sensing," Adv. Opt. Photon. **2**, 370–404 (2010).

[20] O. Kenji, "Semiconductor ring laser gyro," Japanese Patent # JP 60,148,185 (1985).

[21] C. Ji, M. H. Leary, and J. M. Ballantyne, "Long wavelength triangular ring laser," IEEE Photonic. Tech. Lett. **9**, 1469–1471 (1997).

[22] R. van Roijen, E. C. M. Pennings, M. J. N. van Stalen, T. van Dongen, B. H. Verbeek, and J. M. M. van der Heijden, "Compact InP-based ring lasers employing multimode interference couplers and combiners," Appl. Phys. Lett. **64**, 1753–1755 (1994).

[23] T. Krauss, R. M. De La Rue, and P. J. R. Laybourn, "Impact of output coupler configuration on operating characteristics of semiconductor ring lasers," J. Lightwave Technol. **13**, 1500–1507 (1995).

[24] M. Sorel, P. J. R. Laybourn, A. Scirè, S. Balle, G. Guiliani, R. Miglierina, and S. Donati, "Alternate oscillations in semiconductor ring lasers," Opt. Lett. **27**, 1992–1994 (2002).

[25] H. Cao, H. Ling, C. Liu, H. Deng, M. Benavidez, V. A. Smagley, R. B. Caldwell, et al. "Large S-section-ring-cavity diode lasers: directional switching, electrical diagnostics, and mode beating spectra," IEEE Photonic. Tech. Lett. **17**, 282–284 (2005).

[26] J. P. Hohimer, and G. A. Vawter, "Unidirectional semiconductor ring lasers with racetrack cavities," Appl. Phys. Lett. **63**, 2457–2459 (1993).

[27] M. N. Armenise, C. Ciminelli, F. De Leonardis, and V. M. N. Passaro, "Quantum effects in new integrated optical angular velocity sensors," in *Proceedings to the 5th International Conference on Space Optics*, 595–597 (ESA, Noordwijk, 2004).

[28] G. L. Vossler, M. D. Olinger, and J. L. Page, "Solid medium optical ring laser," United States Patent US005408492A (1995).

[29] M. Armenise, *Study and design of an integrated optical sensor for miniaturized gyroscopes for space applications* (Master's degree thesis, Bari Polytechnic, 1997).

[30] M. Armenise, and P. J. R. Laybourn, "Design and Simulation of a Ring Laser for Miniaturised Gyroscopes," Proc. SPIE **3464**, 81–90 (1998).

[31] P. J. R. Laybourn, *Integrated optoelectronics application in space* (ESA International Workshop on Innovation for Competitiveness, Annex I, Noordwijk, 19–21 March 1997).

[32] S. Donati, G. Giuliani, and M. Sorel, "Proposal of a new approach to the electrooptical gyroscope: the GaAlAs integrated ring laser," Alta Freq. **9**, 61–63 (1997).

[33] M. Sorel, P. J. Laybourn, G. Giuliani, and S. Donati, "Progress on the GaAlAs ring laser gyroscope," Alta Frequenza - Rivista Di Elettronica **10**, 45–48 (1998).

[34] P. J. R. Laybourn, M. Sorel, G. Giuliani, and S. Donati, "Integrated semiconductor laser rotation sensors," Proc. SPIE **3620**, 322–331 (1999).

[35] K. Taguchi, K. Fukushima, A. Ishitani, and M. Ikeda, "Proposal of a semiconductor ring laser gyroscope," Opt. Quant. Electron. **31**, 1219–1226 (1999).

[36] T. Numai, "Analysis of signal voltage in a semiconductor ring laser gyro," IEEE J. Quantum Elect. **36**, 1161–1167 (2000).

[37] M. N. Armenise, M. Armenise, V. M. N. Passaro, F. De Leonardis, "Integrated optical angular velocity sensor," European Patent EP1219926B1 (2000).

[38] M. Osiński, H. Cao, C. Liu, and P. G. Eliseev, "Monolithically integrated twin ring diode lasers for rotation sensing applications," J. Cryst. Growth **288**, 144–147 (2006).

[39] J. Scheuer, "Direct rotation-induced intensity modulation in circular Bragg micro-lasers," Opt. Express **15**, 15053–15059 (2007).

[40] S. Ezekiel, and S. R. Balsamo, "Passive ring resonator laser gyroscope," Appl. Phys. Lett. **30**, 478–480 (1977).

[41] R. Adar, M. R. Serbin, and V. Mizrahi, "Less than 1 dB per meter propagation loss of silica waveguides measured using a ring resonator," J. Lightwave Technol. **12**, 1369–1372 (1994).

[42] M. C. Tien, J. F. Bauters, M. J. R. Heck, D. T. Spencer, D. J. Blumenthal, and J. E. Bowers, "Ultra-high quality factor planar Si_3N_4 ring resonators on Si substrates," Opt. Express **19**, 13551–13556 (2011).

[43] D. T. Spencer, Y. Tang, J. F. Bauters, M. J. R. Heck, and J. E. Bowers, "Integrated Si_3N_4/SiO_2 ultra high Q ring resonators,' in *Proceedings to the IEEE Photonics Conference (ICP)*, 141–142, (IEEE, Burlingame, 2012).

[44] C. Vannahme, H. Suche, S. Reza, R. Ricken, V. Quiring, and W. Sohler, "Integrated optical Ti:LiNb03 ring resonator for rotation rate sensing", in *Proceedings to the 13th European Conference on Integrated Optics*, WE1 (IEEE, Copenhagen, 2007).

[45] J. T. A. Carriere, J. A. Frantz, S. Honkanen, R. K. Kostuk, B. R. Youmas, and E. A. J. Vikjaer, "An integrated optic gyroscope using ion-exchanged waveguides," in *Proceedings to the 16th Annual Meeting of the IEEE Lasers and Electro-Optics Society*, 99–100 (IEEE, Tucson, 2003).

[46] G. Li and K. A. Winick, "Integrated optical ring resonators fabricated by silver ion-exchange in glass", in *Proceedings to the IEEE/OSA Conference on Lasers and Electro-Optics/International Quantum Electronics Conference and Photonic Applications Systems Technologies*, CWA63 (Optical Society of America, San Francisco, 2004).

[47] W. Bogaerts, P. de Heyn, T. Van Vaerenbergh, K. de Vos, S. K. Selvaraja, T. Claes, P. Dumon, et al., "Silicon microring resonators," Laser Photonics Rev. **6**, 47–73 (2013).

[48] J. K. S. Poon, L. Zhu, G. A. DeRose, and A. Yariv, "Polymer microring coupled-resonator optical waveguides," J. Lightwave Technol. **24**, 1843–1849 (2006).

[49] F. Dell'Olio, C. Ciminelli, M. N. Armenise, F. M. Soares, and W. Rehbein, "Design, fabrication, and preliminary test results of a new InGaAsP/InP high-Q ring resonator for gyro applications," in *Proceedings to the IEEE International Conference on Indium Phosphide and Related Materials*, 124–127 (IEEE, Santa Barbara, 2012).

[50] C. Ciminelli, F. Dell'Olio, M. N. Armenise, F. M. Soares, and W. Passenberg, "High performance InP ring resonator for new generation monolithically integrated optical gyroscopes," Opt. Ex-

press **21**, 556–564 (2013).

[51] C. Ciminelli, F. Peluso, and M. N. Armenise, "A new integrated optical angular velocity sensor," Proc. SPIE **5728**, 10.1117/12.590421 (2005).

[52] H. K. Hsiao, and K. A. Winick, "Planar glass waveguide ring resonators with gain," Opt. Express **15**, 17783–17797 (2007).

[53] H. Lee, T. Chen, J. Li, K. Y. Yang, S. Jeon, O. Painter, and K. J. Vahala, "Chemically etched ultrahigh-Q wedge-resonator on a silicon chip," Nat. Photonics **6**, 369–373 (2012).

[54] X. Zhang, and A. M. Armani, "Silica microtoroid resonator sensor with monolithically integrated waveguides," Opt. Express **21**, 23592–23603 (2013).

[55] C. Ford, R. Ramberg, K. Johnson, W. Berglund, B. Ellerbusch, R. Schermer, and A. Gopinath, "Cavity element for resonant micro optical gyroscope," IEEE Aero. El. Sys. Mag. **15**, 33–36 (2000).

[56] X. L. Zhang, and K. J. Zhou, "Open-loop experiments of resonator micro-optic gyro," Optoelectron. Lett. **5**, 97–100 (2009).

[57] H. Yu, C. Zhang, L. Feng, Z. Zhou, L. Hong, "SiO_2 waveguide resonator used in an integrated optical gyroscope," Chinese Phys. Lett. **26**, 054210 (2009).

[58] L. Guo, B. Shi, C. Chen, and M. Zhao, "A large-size SiO_2 waveguide resonator used in integration optical gyroscope," Optik **123**, 302–305 (2012).

[59] M. Zhao, B. R. Shi, C. Chen, L. J. Guo, R. Zhang, Q. Zhang, "Experimental study on resonator micro optic gyroscope," Proc. SPIE **8191**, 10.1117/12.900776 (2011).

[60] K. Iwatsuki, M. Saruwatari, M. Kawachi, and H. Yamazaki, "Waveguide-type optical passive ring-resonator gyro using time-division detection scheme," Electron. Lett. **25**, 688–689 (1989).

[61] H. Ma, Y. Yan, Y. Chen, and Z. Jin, "Improving long-term stability of a resonant micro-optic gyro by reducing polarization fluctuation," IEEE Photon. J. **4**, 2372–2381 (2012).

[62] H. Ma, Z. He, and K. Hotate, "Reduction of backscattering induced noise by carrier suppression in waveguide-type optical ring resonator gyro," J. Lightwave Technol. **29**, 85–90 (2011).

[63] K. Suzuki, K. Takiguchi, and K. Hotate, "Monolithically integrated resonator microoptic gyro on silica planar lightwave circuit," J. Lightwave Technol. **18**, 66–72 (2000).

[64] K. Hotate, K. Takiguchi, A. Hirose, "Adjustment-free method to eliminate the noise induced by the backscattering in an optical passive ring-resonator gyro," IEEE Photonic. Tech. Lett. **2**, 75–77 (1990).

[65] H. Mao, H. Ma, and Z. Jin, "Polarization maintaining silica waveguide resonator optic gyro using double phase modulation technique," Opt. Express **19**, 4632–4643 (2011).

[66] L. Feng, M. Lei, H. Liu, Y. Zhi, and J. Wang, "Suppression of back-reflection noise in a resonator integrated optic gyro by hybrid phase-modulation technology," Appl. Optics **52**, 1668–1675 (2013).

[67] H. Ma, S. Wang, and Z. Jin, "Silica waveguide ring resonators with multi-turn structure," Opt. Commun. **281**, 2509–2512 (2008).

[68] C. Ciminelli, F. Dell'Olio, M. N. Armenise, "High-Q spiral resonator for optical gyroscope applications: numerical and experimental investigation," IEEE Photon. J. **4**, 1844–1854 (2012).

[69] H. Y. Yu, C. X. Zhang, L. S. Feng, L. F. Hong, and J. J. Wang, "Optical noise analysis in dual-resonator structural micro-optic gyro," Chinese Phys. Lett. **28**, 084203 (2011).

[70] C. Ciminelli, C. E. Campanella, M. N. Armenise, "Optical rotation sensor as well as method of manufacturing an optical rotation sensor," European Patent EP056933 (2013).

[71] H. Ma, W. Wang, Y. Ren, and Z. Jin, "Low-noise low-delay digital signal processor for resonant micro optic gyro," IEEE Photonic. Tech. Lett. **25**, 198–201 (2013).

[72] M. Lei, L. Feng, and Y. Zhi, "Sensitivity improvement of resonator integrated optic gyroscope by double-electrode phase modulation," Appl. Optics **52**, 7214–7219 (2013).

[73] C. Ciminelli, V. M. N. Passaro, F. Dell'Olio, and M. N. Armenise, "Quality factor and finesse optimization in buried InGaAsP/InP ring resonators," J. Europ. Opt. Soc. Rap. Public. **4**, 09032 (2009).

[74] H. Ma, X. Chang, H. Mao, and Z. Jin, "Laser frequency noise limited sensitivity in a resonator optic gyroscope," in *Proceedings to the 15th OptoElectronics and Communications Conference*, 706–707 (IEEE, Sapporo, 2010).

[75] Z. Jin, G. Zhang, H. Mao, and H. Ma, "Resonator micro optic gyro with double phase modulation technique using an FPGA-based digital processor," Opt. Commun. **285**, 645–649 (2012).

[76] C. Peng, Z. Li, and A. Xu, "Optical gyroscope based on a coupled resonator with the all-optical analogous property of electromagnetically induced transparency," Opt. Express **15**, 3864–3875 (2007).

[77] C. Peng, Z. Li, and A. Xu, "Rotation sensing based on a slow light resonating structure with high group dispersion," Appl. Optics **46**, 4125–4131 (2007).

[78] J. Scheuer, and A. Yariv, "Sagnac effect in coupled-resonator slow-light waveguide structures," Phys. Rev. Lett. **96**, 053901 (2006).

[79] Y. Zhang, H. Tian, X. Zhang, N. Wang, J. Zhang, H. Wu, and P. Yuan, "Experimental evidence of enhanced rotation sensing in a slow-light structure," Opt. Lett. **35**, 691–693 (2010).

[80] Y. Zhang, N. Wang, H. Tian, H. Wang, W. Qiu, J. Wang, P. Yuan, "A high sensitivity optical gyroscope based on slow light in coupled-resonator-induced transparency," Phys. Lett. A **372**, 5848–5852 (2008).

[81] M. A. Terrel, M. J. F. Digonnet, and S. Fan "Performance limitations of a coupled resonant optical waveguide gyroscope," J. Lightwave Technol. **27**, 47–54 (2009).

[82] J. R. E. Toland, Z. A. Kaston, C. Sorrentino, and C. P. Search, "Chirped area coupled resonator optical waveguide gyroscope," Opt. Lett. **36**, 1221–1223 (2011).

[83] C. Sorrentino, J. R. E. Toland, and C. P. Search, "Ultra-sensitive chip scale Sagnac gyroscope based on periodically modulated coupling of a coupled resonator optical waveguide," Opt. Express **20**, 354–363 (2011).

[84] C. Ciminelli, C. E. Campanella, F. Dell'Olio, C. M. Campanella, and M. N. Armenise, "Theoretical investigation on the scale factor of a triple ring cavity to be used in frequency sensitive resonant gyroscopes," J. Europ. Opt. Soc. Rap. Public **8**, 13050 (2013).